Rate-induced transitions and advanced takeoff in power systems

Cite as: Chaos **30**, 061103 (2020); https://doi.org/10.1063/5.0002456
Submitted: 25 January 2020 . Accepted: 22 May 2020 . Published Online: 09 June 2020

K. S. Suchithra, E. A. Gopalakrishnan, Elena Surovyatkina, and Jürgen Kurths

Chaos ARTICLE scitation.org/journal/cha

Rate-induced transitions and advanced takeoff in power systems

Cite as: Chaos **30**, 061103 (2020); doi: 10.1063/5.0002456
Submitted: 25 January 2020 · Accepted: 22 May 2020 ·
Published Online: 9 June 2020

K. S. Suchithra,[1] E. A. Gopalakrishnan,[1,a)] Elena Surovyatkina,[2,3] and Jürgen Kurths[2,4]

AFFILIATIONS

[1]Center for Computational Engineering & Networking (CEN), Amrita School of Engineering, Coimbatore, Amrita Vishwa Vidyapeetham, India
[2]Potsdam Institute for Climate Impact Research, Potsdam 14473, Germany
[3]Space Research Institute of Russian Academy of Sciences, Moscow 117810, Russia
[4]Department of Physics, Humboldt University of Berlin, Newtonstrasse 15, Berlin 12489, Germany

[a)]**Author to whom correspondence should be addressed:** ea_gopalakrishnan@cb.amrita.edu

ABSTRACT

One of the most common causes of failures in complex systems in nature or engineering is an abrupt transition from a stable to an alternate stable state. Such transitions cause failures in the dynamic power systems. We focus on this transition from a stable to an unstable manifold for a rate-dependent mechanical power input via a numerical investigation in a theoretical power system model. Our studies uncover early transitions that depend on the rate of variation of mechanical input. Furthermore, we determine the dependency of a critical rate on initial conditions of the system. Accordingly, this knowledge of the critical rate can be used in devising an effective control strategy based on artificial intelligence (AI).

Blackout is the short-term loss of the ability of a power grid to deliver reliable electric power supply. The global trend toward urbanization leads to an increase in demand for electric power that magnifies the challenge of controlling blackout. There are many causes for the power system failures, which can lead to a blackout. Often, our electric power system operates close to the stability margin, which significantly magnifies the chance of cascading failures in the presence of disturbances. The stability analysis conducted hitherto in the power system confined to either linear or nonlinear stability analysis by considering the power system as an autonomous system. However, the power system is a non-autonomous system in which parameters are time-dependent. In this paper, we study the rate-dependent variation of the control parameter and rate-induced transition in a mathematical model of the power system. As the transition will result in power system instability, leading to interruption of the supply and a massive loss of revenue, studying factors leading to transition is highly essential.

I. INTRODUCTION

The essential infrastructure services for mankind ranging from drinking water to oil sector and from telecommunications to banking rely on electric power systems. Therefore, the electric power system is a crucial infrastructure for the progress of society.[1] Although significant attention has been paid to ensure reliable and robust power supply, power outages remain as a gnawing issue. A majority of the power system blackouts of large networks such as the Northeastern U.S. blackout in 2003 and the 2012 blackout in India are identified as sudden transitions from stable to unstable operating regimes.[2] Therefore, stability analysis of the power system is essential for ensuring the reliability of power supply and maintaining the power quality.

Subject to the nature and severity of the disturbances, power system stability is of two types, small-signal stability and transient stability.[3] Small-signal stability of a power system is the ability to attain a new equilibrium position after a small change in the power or disturbance of less severity. In contrast, transient stability is the

ability to reach a stable state following a severe disturbance such as short circuits, a sudden outage of a generator, or a loss of line. However, both transient and steady-state instabilities finally manifest into the loss of synchronism and voltage instability.[3] Voltage instability is the progressive decline of voltage at the system buses, ultimately leading to voltage collapse, while the loss of synchronism is the result of rotor angle instability. As voltage and synchronous instability trigger cascading failures, wherein sequential tripping of generators and transmission lines are involved, these instabilities are referred to as critical transitions (CTs) in power systems.[4] Hence, it is imperative to identify the factors leading to sudden and irreversible transitions in power systems.

The benchmark works on power system instability were carried out in mathematical models of the power system[3] by linearizing the dynamics involved. Menck *et al.* reported that the linearization based approach to analyze stability is too local and is insufficient to assess the stability of the system. Menck *et al.* stressed the need for adopting nonlinear analytical techniques to determine the stability of systems having multiple stable states.[5] Ma *et al.* identified that the power system is a bi-stable system, which exhibits the co-existence of two stable states.[6] The stability of bi-stable systems depends upon both the system state and the initial conditions.[7] The transient instability of the power system involves large excursions of generator rotor angles and power swings, which may result in the crossing of stability boundaries of co-existing stable states. The bi-stable nature of the power system model necessitates the nonlinear stability analysis to capture the stability map of power systems.[8]

The nonlinear stability of power systems is usually analyzed using perturbation techniques and bifurcation theory.[9,10] However, due to the dependence of small parameter assumptions associated with perturbation techniques,[9] bifurcation techniques are widely accepted for a nonlinear stability analysis of power systems.[10,11] Bifurcation is the sudden qualitative change observed in a dynamic system to the infinitesimal variation of the control parameter.[7] The ever-increasing power demand at the customer side followed by sudden and irreversible transitions in the operating state of the system is termed as bifurcation induced transitions.[12] The bifurcation studies of power system models consider the quasi-static variation of real and reactive power demands.[10,11] Dobson demonstrated a Saddle-Node Bifurcation (SNB), leading to voltage collapse on a simple three bus system with a static load. Ajjarappu and Lee replaced the static load in the three bus power system model[11] by an induction machine load and reported the occurrence of oscillatory solutions leading to the Hopf bifurcation and later to voltage collapse. Furthermore, multi-parameter bifurcation analysis in power system models investigates the problem of voltage instability in detail in distributed systems.[13] However, another contemporary issue, rotor angle instability, has been less explored from the perspective of bifurcation theory.

In order to determine the rotor angle instability, Ma *et al.* performed bifurcation studies in a Single Machine Infinite Bus (SMIB) for different damping values ranging from negative to positive.[6] The authors identified the presence of fixed points and limit cycle, which corresponds to stable and unstable operating regimes in a power system. The bifurcation analysis hitherto in a power system studied the quasi-static variation of the control parameter, assuming the system as autonomous. However, the modern power system is non-autonomous due to the perpetual changes in load and generation. These changes are the consequence of the uncertainties imposed by renewable resources.

Cloud passing in Photo Voltaic (PV) and wind gust in wind energy are the key challenges contributing to uncertainties in renewable generation. Consequently, renewable generation demands faster Turbine Governor Control (TGC) compared to the conventional generation. The PV generation varies as fast as 63% of rated capacity/min against the desired limit of 30% of rated capacity/min. The unsteady generation, along with fast load changes, presents a formidable problem toward the aim of 80% renewable energy.[14] Due to the restrictions on the fast variation of TGC, the conventional practice in a renewable integrated power system is to limit the PV/wind generation within 50% of the maximum capacity. Therefore, immediate attention to the development of safe control strategies and stability analysis of the non-autonomous power system is essential in the context of renewable penetration. Hence, our study on the stability of the canonical non-autonomous power system model is a pertinent problem.

Rate-dependent bifurcations using canonical models of standard bifurcations are available in the literature. Baer *et al.* observed a delay in the transition from a non-oscillatory to an oscillatory state for the system parameter variation as a function of time in a relaxation oscillator.[15] Successively, Majumdar *et al.* established the delay in transition to the other state for the slow variation of the control parameter and the dependence of the delay on initial conditions in nematic liquid crystals.[16] Further, Ashwin *et al.* reported the presence of transitions in climate systems arising out of rates above the critical rates.[17] Subsequently, Tony *et al.* performed the rate-dependent variation of system parameters in a thermoacoustic system and investigated the transitions induced solely due to the rate-dependent variation of system parameters within the bistable region.[18] The studies on the aforesaid dynamical systems establish that the stability regimes of the autonomous and non-autonomous systems are different.

Suchithra and Gopalakrishnan reported the delay in transitions from a stable state to an alternate stable state for the variation of mechanical power as a function of time in a power system model.[19] The contribution of this paper is to propose a dynamic bifurcation analysis of the power system for the linear variation of mechanical power and to analyze the stability of the non-autonomous power system model. To the best of our knowledge, dynamic bifurcation analysis, which preserves the non-autonomous nature, is unexplored in the power system so far.

A complete investigation of rate-dependent transitions and its impact on stability in high dimensional power systems is strenuous due to the complexity of the system. In order to avoid this difficulty, we adopt a canonical system that retains the essential features of the power system to inspect the stability, while maintaining simplicity for a detailed analysis. SMIB is a lumped parameter representation of the actual power grid, widely adopted for stability analysis of power systems.[8] Therefore, we adopt the canonical power system model, commonly used for stability analysis for our numerical investigation. The model consists of a single generator node and neglects the ohmic resistance, which is negligible compared to the susceptance of the high voltage transmission lines. However, this assumption is not

valid in a distribution network since both resistance and susceptance are compatible.[20]

The organization of the paper is as follows. We describe the canonical power system model adopted to study the dynamical behavior of the system in Sec. II. Section III analyzes the transitions in the power system model by determining the dynamic bifurcation diagram. Finally, the conclusions are presented in Sec. IV.

II. MATHEMATICAL MODEL OF THE POWER SYSTEM

We carry out mathematical modeling of the power system swing equation in this section. The swing equation analysis is widely used to assess the stability of power systems.[8,21] We also derive an analytical solution for demonstrating the transition that occurs in the power system model. The generator angle dynamics is depicted as

$$M\ddot{\delta} + D\dot{\delta} = P_m - P_e, \tag{1}$$

where

$$P_e = \frac{EV\sin(\delta)}{X}, \tag{2}$$

$$T_{d0}\dot{E} = E_f - \frac{E(x_d\prime\Sigma + (x_d - x_d\prime)) + V\sin\delta}{x_d\prime\Sigma}. \tag{3}$$

Here, M denotes the inertia constant, and D is the damping factor. D represents the overall damping effect of all the elements that contribute toward damping in the physical system. P_m and P_e, respectively, represent the mechanical power input and the electrical power output. δ represents rotor angular displacement with respect to the synchronous reference axis. Here, E is the generator induced electromotive force (emf), which is governed by Eq. (3), whereas V is the terminal voltage of the infinite bus. In a power system, δ is the phase shift between the voltage vector of the infinite bus and the generated voltage. ω is the deviation in the angular velocity from that of the reference frame. The reference frame is assumed to rotate at a constant synchronous velocity of ω_s. x_d and $x_d\prime$ are direct axis synchronous and transient reactance, T_{d0} is the direct axis open circuit time constant, and E is the internal flux decay.[6] Furthermore, we introduce the following reductions:

$$X\prime = x_d - x_d\prime, \quad B = \frac{1}{x_d\prime\Sigma}.$$

We fix standard values for the rest of the parameters as[6,8]

$$M = 0.3, \quad B = 1, \quad T_{d0} = 2,$$
$$D = 0.2, \quad E_f = 1, \quad x_d\prime\Sigma = 1.$$

The system dynamics in terms of the normalized parameters[6] is

$$\dot{\delta} = \omega, \tag{4}$$

$$\dot{\omega} = -3.33E\sin\delta - 0.66\omega + 3.33P_m, \tag{5}$$

$$\dot{E} = 0.5\cos\delta - E + 0.5. \tag{6}$$

We have the system dynamics represented in terms of the state variables, $[\delta\ \omega\ E]$. From Eqs. (4)–(6), we conclude that the transitions in the dynamics are due to the variation of P_m since the rest of the parameters are fixed. According to Eqs. (4)–(6), we get the equilibrium points upon solving the algebraic equations as in (7)–(9),

$$\omega = 0, \tag{7}$$

$$-3.33E\sin\delta - 0.66\omega + 3.33P_m = 0, \tag{8}$$

$$0.5\cos\delta - E + 0.5 = 0. \tag{9}$$

The complexity of Eqs. (7)–(9) makes finding out an explicit expression for δ_0 and E_0 difficult. Simplifying Eqs. (8) and (9), the equilibrium points can be obtained in terms of P_m as

$$P_m = \frac{1}{2}\left[\frac{1}{2}\sin(2\delta) + \sin(\delta)\right], \tag{10}$$

$$E = \frac{1}{2}\left(1 + \cos(\delta)\right). \tag{11}$$

We determine the Jacobian J of the system to analyze the stability of the equilibrium points as follows:

$$J = \begin{bmatrix} 0 & 1 & 0 \\ -3.33E_0\cos\delta_0 & -0.66 & -3.33\sin\delta_0 \\ -0.5\sin\delta_0 & 0 & -1 \end{bmatrix}. \tag{12}$$

We evaluate the trace, τ and the determinant, Δ of the Jacobian matrix as

$$\tau = -1.66, \quad \Delta = 3.33\left[\frac{1}{2}\sin\delta_0^2 - E_0\cos\delta_0\right].$$

The value of τ remains constant as the damping is not varied. Therefore, the stability of the equilibrium points of the system is determined by P_m. Substituting for Δ in terms of P_m for analyzing the nature of the fixed points, we get the following expression:

$$\Delta = 3.33\left[\frac{P_m^2}{2E^2} - \left(\frac{1 - \frac{P_m^2}{E^2} - \sqrt{1 - \frac{P_m^2}{E^2}}}{2}\right)\right], \tag{13}$$

where

$$\sin\delta_0 = \frac{P_m}{E}, \quad E_0 = \frac{1 + \sqrt{1 - \frac{P_m^2}{E^2}}}{2}. \tag{14}$$

The system is having fixed points when Δ is real and no fixed point when Δ is imaginary.[7] The determinant becomes an imaginary number when $\frac{P_m}{E} > 1$. As we increase P_m, Δ becomes imaginary when P_m just crosses E, leading to vanishing of the fixed points.[7] Figure 1(c) shows the point at which no fixed point exists. The P_m value at which the fixed points disappear is a point of CT in the forward path denoted as P_{mCT1}.

We solve the characteristic equation of the system to obtain the nature of the equilibrium point. Upon solving the characteristic

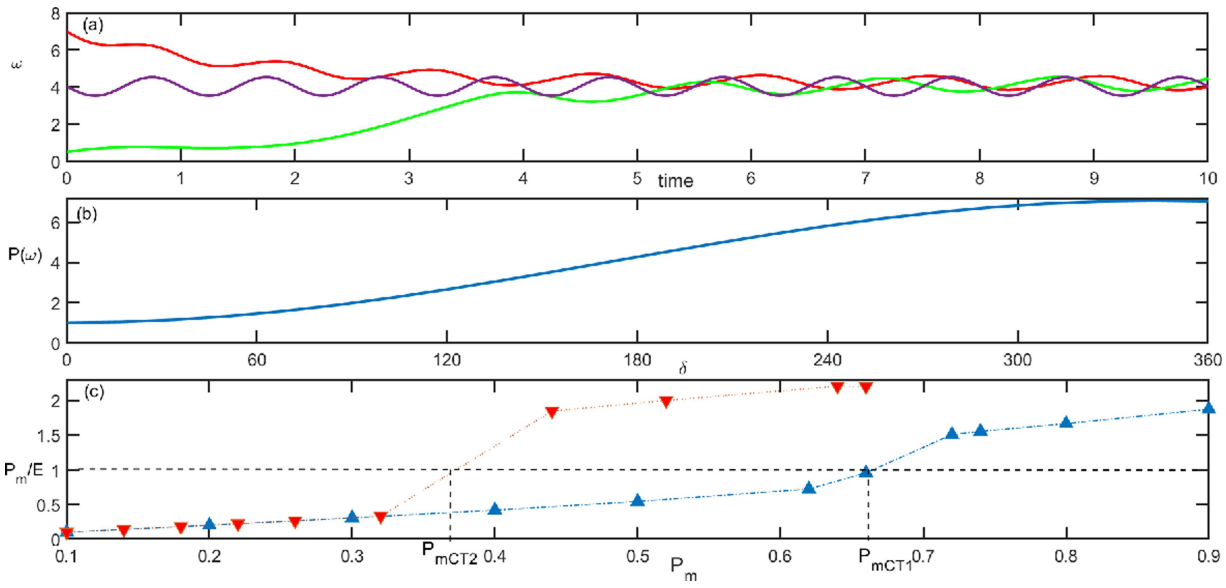

FIG. 1. (a) Trajectories of ω converging to a nullcline for $P_m > P_{mCT1}$: the curve in lavender color indicates the nullcline of the system depicted by Eq. (16); the trajectory in red color shows the convergence of a system trajectory from a high initial condition to the nullcline; the green trajectory demonstrates ω starting from a low value converging to the nullcline. (b) Poincaré map traversing from $\delta = 0$ to $\delta = 2\pi$ within the rectangular box. (c) The figure depicts the variation of P_m/E for P_m illustrating the flux decay for increments in P_m corresponding to the initial conditions within the basin of attraction of the fixed point as the blue color curve, whereas initial conditions that belong to the basin of attraction of the limit cycle are shown in the coral color curve. The value at which these curves cross the horizontal line of magnitude 1 is the points of CT in the forward and reverse path, respectively.

equation,

$$\lambda^3 + 1.66\lambda^2 + \lambda(0.66 + 3.33E_0\cos\delta_0) + 3.33[E_0\cos\delta_0 - 0.5\sin^2\delta_0] = 0, \quad (15)$$

we get three eigenvalues, of which one is a pair of complex conjugates with a negative real part and the third is real, and negative. The nature of the eigenvalues indicates that the fixed point is a focus node.[22]

We adopted a strategy similar to the analysis of a forced oscillator in order to inspect the system behavior upon crossing P_{mCT1}.[7] We consider the nullcline of ω presented in Fig. 1(a) for $P_m > P_{mCT1}$. It is established that nullcline is the set of points, where all the trajectories of ω asymptotically converge.[7] The nullcline is presented for $P_m = 0.9$ such that P_m is greater than P_{mCT1} for nullcline,[7]

$$\omega = \frac{3.33}{0.66}[P_m - E\sin\delta]. \quad (16)$$

Analysis of the phase space of the system reveals the long term behavior of the system. We confine our investigation within a rectangular box where δ ranges from $[0\ 2\pi]$ and ω varies from a lower bound below the nullcline to an upper bound above the nullcline as shown in Fig. 1(b) since the limits are sufficient to analyze the asymptotic behavior. Consider $P(\omega)$, which is a trajectory in cylindrical coordinates. The trajectory illustrates us how the height of a trajectory $P(\omega)$ changes after one lap around the cylinder (δ, ω). Figure 1(b) depicts the trajectory $P(\omega)$ traversing from ω_1 to ω_2. If $P(\omega)$ is such that $P(\omega) = \omega$, then it indicates the existence of a periodic orbit.[7] Figure 1(a) shows that trajectories of ω above the nullcline travel downwards to the nullcline, whereas trajectories of ω below the nullcline traverse upwards. Therefore, the considered $P(\omega)$ is a monotonic function. It is evident that the long term behavior of the system when $P_m > P_{mCT1}$ will be a CT from a focus node to limit cycle oscillations. As P_m is decreased from values above P_{mCT1} asymptotically, Δ changes from imaginary to real upon crossing a threshold value $P_m = P_{mCT2}$. As we decrease P_m, the amplitude of the limit cycle oscillations get reduced, leading to vanishing of limit cycle oscillations at P_{mCT2}, which is known as the fold point.

The differential equations are solved using the standard fourth-order Runge–Kutta scheme with a fixed step size of 0.01. The integration step size is sufficiently small compared to the time of transient response, which is of the order of tens of seconds.[3]

III. TRANSITIONS IN A POWER SYSTEM MODEL

The rotor angle instability of a synchronous machine occurs through a critical transition (CT) in an angular velocity. Therefore, we study the CT with respect to the angular velocity in a power system model to identify the chances of rotor angle instability. Initially, we perform the quasi-static bifurcation studies, wherein we consider the power system as an autonomous system. Furthermore, we allow the system parameter to evolve as a function of time to preserve the non-autonomous nature of the power system.

A. Quasi-static bifurcation diagram

We record the root mean square (RMS) value of the response of the angular velocity, $\omega\prime$ by varying the non-dimensional mechanical power P_m, quasi-statically. We observe an abrupt increase in the amplitude of $\omega\prime$ along with an oscillatory response, when P_m is increased above the first critical value P_{mCT1}(indicated as I in Fig. 2). Figure 3 shows the time series and phase space of the system before and after crossing the critical value, P_{mCT1}. It is clear from Fig. 3(a) and (b) that the equilibrium point corresponds to a focus node prior to crossing P_{mCT1}.[22] Upon crossing P_{mCT1}, the system enters a state of stable oscillations. The time series and phase space shown in Figs. 3(c) and 3(d) demonstrate the presence of stable oscillations.

Furthermore, we alter the operating conditions of the system and reduce P_m to obtain the second critical value, which marks the reverse transition from the oscillatory state to the non-oscillatory state. We observe that the reverse transition occurs at a later point, P_{mCT2}. In short, at P_{mCT1}, the focus-node equilibrium points undergoes a bifurcation [as represented by (*I*) in the bifurcation diagram], and the system transits from the non-oscillatory state to a stable limit cycle; the reverse transition occurs via the Saddle-Node bifurcation [denoted by (*III*) in the bifurcation diagram] at the second critical point P_{mCT2}. The presence of two critical points in the bifurcation diagram reveals the existence of a bi-stable region in the system.[7]

In a bi-stable region, the system is linearly stable. However, the system can be forced into the other state if the initial conditions fall above some threshold.[23] Specifically, a bi-stable region is one in which the system occupies either of the two states, depending upon the initial conditions.[7] For a power system exhibiting the co-existence of two stable states, a transient disturbance may trigger a transition from a non-oscillatory to an oscillatory state,[5] which is strong enough to trigger a cascading failure and blackout. Bialek has illustrated such a cascading failure that spreads across France, Spain, and Italy triggered by a local failure in Northern Germany.[24] Hence, identifying the basin of attraction of each state gives information about the safe margin of the states against perturbations. The transient disturbances and fluctuations in the power system may trigger the crossing of the basin of attraction of the stable operating state. Therefore, determination of basins of attraction of both the oscillatory and the non-oscillatory states is crucial for maintaining stability. Menck *et al.* explained how basin stability complements linear stability.[5] In contrast, Hasegawa and Ueda performed an investigation on identifying the basin of attraction of the different states in a power system model described by the swing equation.[25]

We perform a numerical experiment as explained below for estimating the basins of attraction of both states. Impulse excitation is given to the system in the ascending order of initial conditions and the maximum value of the operating condition ω_0, for a particular P_m for which the system goes to the non-oscillatory state is recorded. We consider the entire values of P_m within the bi-stable region at an interval of 0.05 to experiment. Furthermore, we repeat the experiment for the same set of values of P_m, but with initial conditions corresponding to the reverse path to determine the minimum value of ω_0 for which the system guarantees stable oscillations. Then, we compute the mean of the recorded maximum and minimum values. The calculated mean is the boundary of the basins of attraction for the stable non-oscillatory and stable oscillatory states of the system.

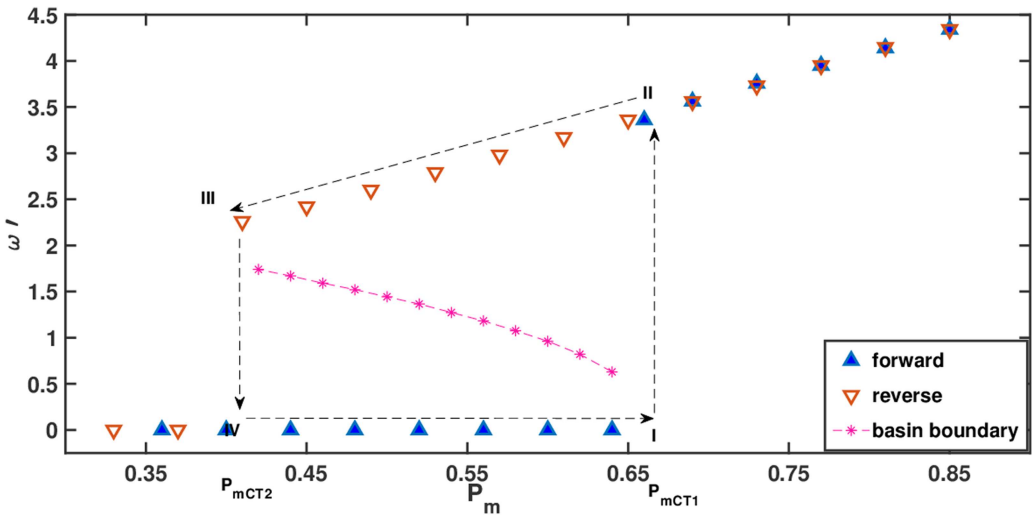

FIG. 2. Bifurcation diagram: The bifurcation diagram depicts the RMS value of the angular velocity $\omega\prime$ for the quasi-static variation of the mechanical power, P_m. The forward transition from the stable non-oscillatory state (lower branch) to the stable oscillatory state (upper branch) occurs at the first critical point $P_{mCT1}(I)$. At P_{mCT1}, the focus-node equilibrium point undergoes a bifurcation, and the system transits from the non-oscillatory state to a stable limit cycle. Upon decreasing P_m, a reverse transition from the stable oscillatory state (upper branch) to the stable non-oscillatory state (lower branch) occurs via Saddle-Node Bifurcation (SNB) at the second critical point, P_{mCT2}. The dotted line demarcates the boundary separating the basin of attraction of a stable non-oscillatory state and a stable oscillatory state. The system can remain in the stable oscillatory or stable non-oscillatory state within the bi-stable region (I–II–III–IV) depending upon the initial conditions. The symbol △ in blue color represents the forward path and the ▽ symbol in red color represents the backward path $P_{mCT1} = 0.66$ and $P_{mCT2} = 0.42$. The initial conditions for the forward and reverse paths, respectively, for the state variables [δ ω E] are [0.2 0.3 0.95] and [1.2 1.5 0.9].

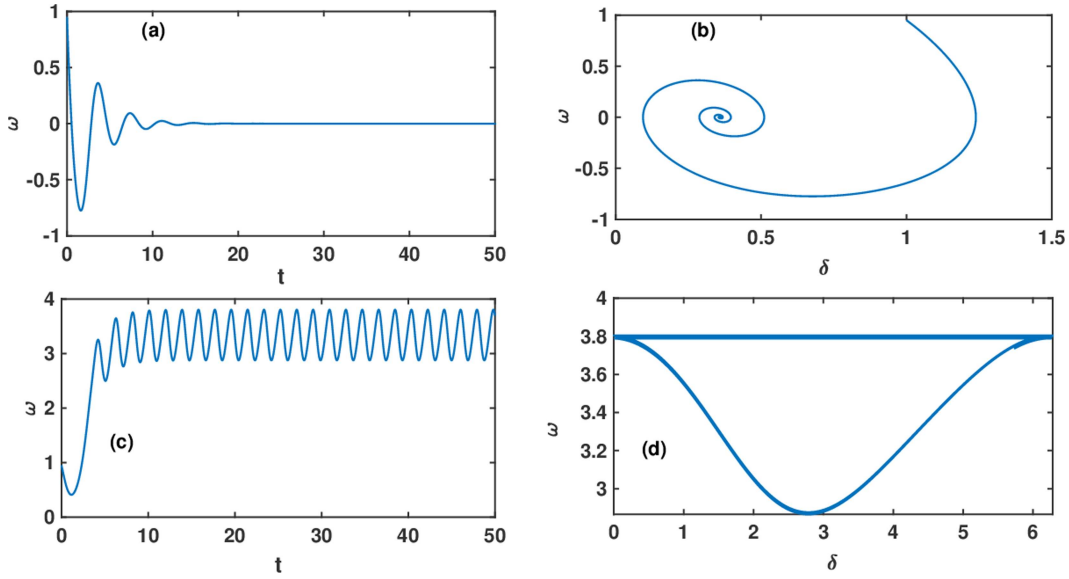

FIG. 3. Time series and the phase space of the system for different mechanical powers. Figs. 3(a) and 3(b), respectively, depict the time series of the state variable angular velocity ω and the phase space of the system in the non-oscillatory state. The mechanical input to the system for the above response is $P_m = 0.34$. The time series of the state variable and the phase space of the system for a mechanical power input of $P_m = 0.74$ are shown in Figs. 3(c) and 3(d), respectively. The initial conditions of the system are given by $\delta = 1$, $\omega = 0.95$, and $E = 1$.

The star symbol demarcates the basin of attraction of the stable non-oscillatory state from the stable oscillatory state in the bifurcation diagram in Fig. 2. In order to compare the stability regimes of the power system as an autonomous and non-autonomous system, we proceed to analyze the stability of the power system as a non-autonomous system in Sec. III B.

B. Rate-induced transitions in the power system

In this section, we vary the mechanical power as a function of time to analyze the transitions in the non-autonomous model of the power system as in Eq. (17). The non-autonomous power system model mimics the frequent variations in generation in the modern power system. It is a common practice in power systems to introduce small linear increments to alter the system conditions gradually.[26,27] Therefore, we perform small linear increments in the mechanical power to the power system model under investigation. The increments in mechanical power are similar to those that occurs in real wind power generation.[28] The small linear increment in mechanical power is to rule out the possibility of severe transient disturbances, which is beyond the scope of the study,

$$P_m{}'(t) = P_{m0} + \mu t. \tag{17}$$

We restrict the variation of the mechanical power between P_{m0} and P_{m1} so that we do not cross P_{mCT1} during our study. Figure 5(a) depicts the time series of the state variable, angular velocity, and the phase space of the system corresponding to the initial value P_{m0} and the final value P_{m1} considered. $P_m{}'(t)$ denotes the variation of mechanical power as a function of time. The figure demonstrates the restriction of P_m within the basin of attraction of the fixed point for the initial conditions given in Fig. 3. Fixing of the mechanical power allows investigating the effect of the rate on inducing transitions to the alternate state. In our study, we maintain the variation of the mechanical power within the standard limits of TGC to mimic the response of the physical system.[28] The above consideration on the rate also eliminates the chances of transitions induced by strong perturbations.

We observe that the system is driven to large amplitude oscillations before the crossing of the first critical point for the rate-dependent variation of the mechanical power. Figure 5(a) shows the variation of the mechanical power as a function of time, and Figs. 5(b) and 5(c) illustrate the corresponding time series of the angular velocity and the phase space of the system. However, we are unable to observe a transition from the non-oscillatory to the oscillatory state for $\mu < 0.001$ for the set of initial conditions described in Fig. 4.

Furthermore, we examine the response of the system shown in Fig. 5 with respect to the quasi-static bifurcation diagram to identify the reason for the early onset of transition to the oscillatory state. Here, we examine the response of the state variable ω for the variation of P_m at the same rate as in Fig. 5 for two different initial conditions. The initial conditions chosen are $\omega = 1.65$ and $\omega = 0.8$. The response seems to decay initially until the curve in yellow color starting from $\omega = 1.65$ cross over the unstable limit cycle and grows toward the stable limit cycle while reaching the final value P_{m1} (Fig. 6). The trajectory in pink color from the initial value $\omega = 0.8$ stays within the basin of attraction of the stable fixed point.

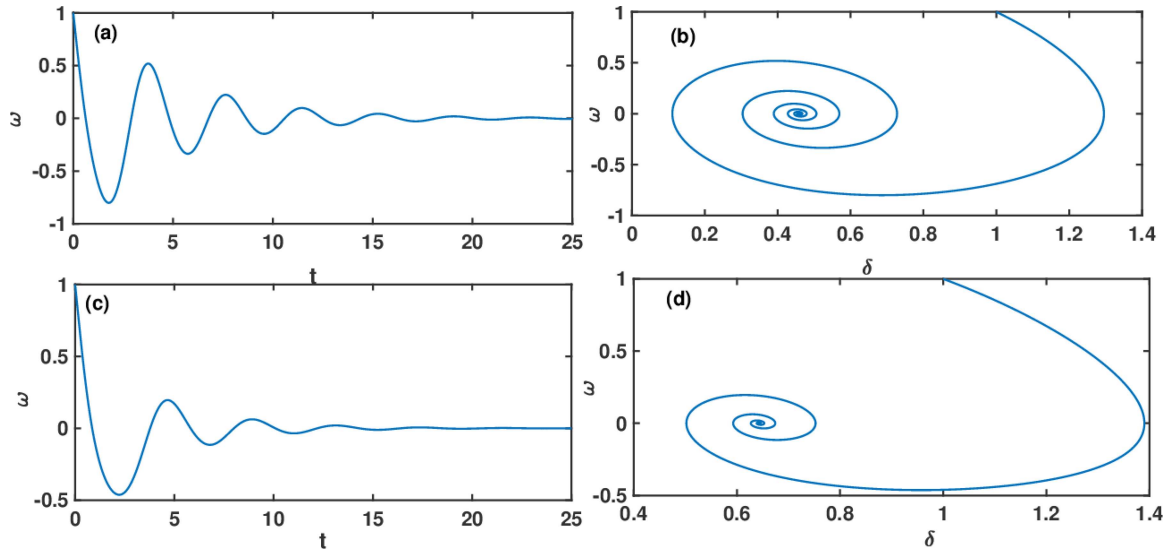

FIG. 4. Time series and the phase space of the system for P_{m0} and P_{mf}. Figure 4(a) depicts the time series of the state variable angular velocity ω, and Fig. 4(b) represents the phase space of the system for $P_m = 0.42$. Figures 4(c) and 4(d) represent the time series of the angular velocity ω and the phase space of the system for $P_m = 0.64$. The initial conditions of the system are the same as the forward path in Fig. 3.

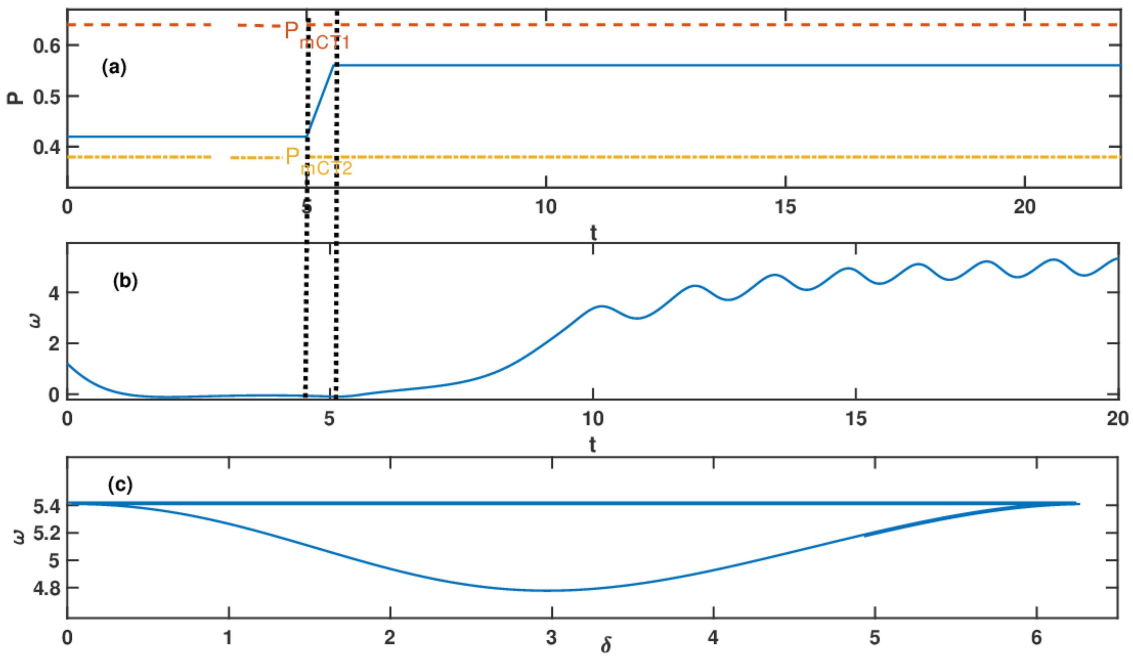

FIG. 5. Rate-induced transitions to oscillatory states. Figure 5(a) depicts the variation of mechanical power P_m as a function of time with $\mu = 0.001$. The dashed line at the top in red color represents the value at which the CT occurs, and the dashed line at the bottom in yellow color indicates the value at which fold bifurcation occurs. Figure 5(b) represents the time series of the state variable angular velocity ω, and Fig. 5(c) represents the phase space of the system in the oscillatory state. The initial conditions of the system are given by $\delta = 0.3$, $\omega = 1.65$, and $E = 0.9$.

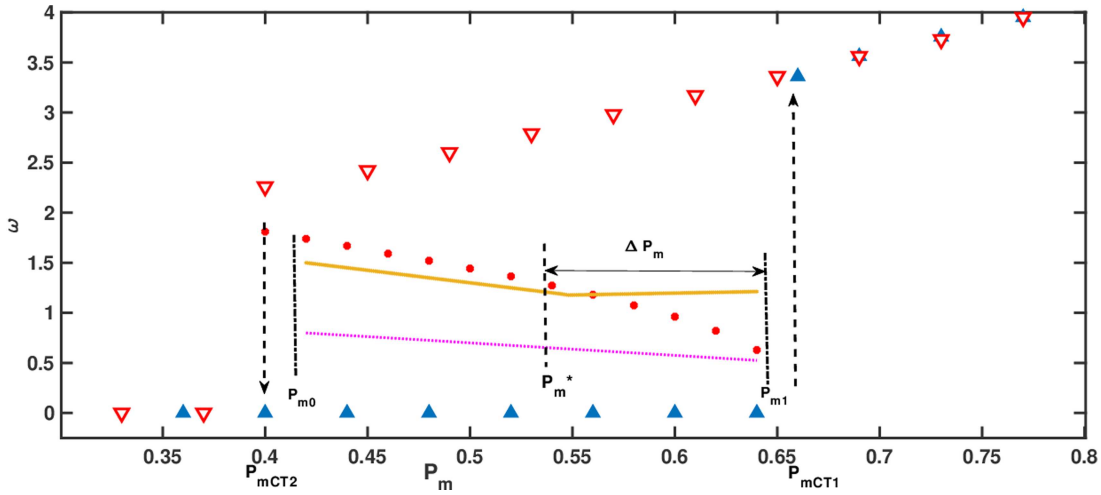

FIG. 6. Rate-induced transitions against quasi-static bifurcation. The figure depicts the RMS value of the state variable ω for the rate-dependent variation of mechanical power from 0.43 to 0.64 for two different initial conditions. The curve starting from the initial condition $\omega = 1.65$ represented in yellow color crosses the unstable limit cycle and grows toward the stable limit cycle. P_m* is the parameter value at which the trajectory crosses the unstable limit cycle. ΔP_m demonstrates the reduction in the stability margin due to the early transition. The second curve, starting from $\omega = 0.8$, depicts the asymptotic decay to the fixed point for the variation of mechanical power at a rate of $\mu = 0.001$.

We infer that the reason for the rate-induced transitions could be the slower decay rate of the system to the basin of attraction of the fixed point compared to the rate of variation of P_m. Moreover, the decay rate is dependent on the initial conditions. Such a feature has been christened "discrete ducks" (*canards discrets*) by Fruchard.[29] Hence, we conclude that the critical rate required for the transition from the stable non-oscillatory state to the unstable oscillatory state is a function of initial conditions.

We term the minimum rate to induce transitions in the system as the critical rate, μ_c. In order to check the dependence of the critical rate upon the initial conditions, the state variable ω is varied

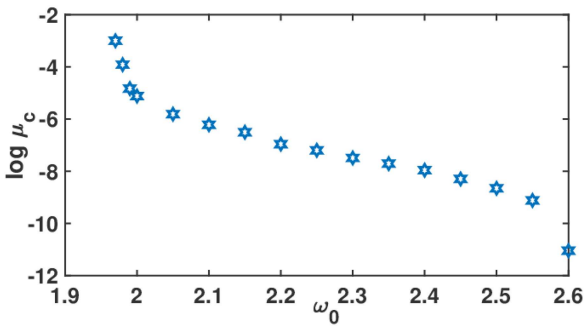

FIG. 7. Critical rate for different initial conditions. This figure depicts the critical rate μ_c required for rate-induced transitions in the theoretical power system model for various initial conditions. The control parameter, P_m, is varied within the bi-stable region at different rates for different initial conditions. Here, ω is varied in the interval [1.97 2.6], and the other state variables δ and E are fixed at 1 and 0.95, respectively.

in the interval [1.97 2.6]. We allow sufficient time for the system to evolve and observe whether the system decays to the fixed point or grows to the limit cycle oscillations. We note down the critical rate at which the system grows toward the limit cycle oscillations for a particular initial condition. We observed that the minimum rate to induce transitions differs as a function of the initial conditions. Figure 7 shows the variation of the critical rate for different initial conditions. We also observe that the system is driven to large amplitude oscillations even for lower rates of variation of the control parameter, upon increasing the initial conditions.

We infer that determination of the critical rate of an operating condition will help in preventing the detrimental transitions. Precisely, this will help in deciding the rate at which the parameter can be safely varied without encountering a catastrophic transition and prevent cascading failures. The rate-induced transitions observed in the power system model and the dependence of the critical rate on the initial conditions are in agreement with the observations reported by Tony *et al.*[18] in thermoacoustic systems. Our results demonstrate a novel route to an understanding of instability in power systems, which is subtle to deal with traditional controllers. Artificial intelligence (AI) has demonstrated impressive growth in applications ranging from image processing[30] to natural language processing over the past decade. Recently, AI-based algorithms have been used for power system control and protection in smart grids.[31,32] Therefore, we recommend AI-based control techniques for power system control.

IV. CONCLUSIONS

We have identified the presence of rate-induced transition in a canonical power system model. We have numerically established that the stable operational regime changes, while considering the

non-autonomous nature of the power system. Further, we have substantiated that the critical rate in inducing transitions to the other state is dependent upon the initial conditions of the system.

Our study is crucial in guaranteeing safe operation, as most of the modern power systems integrated with renewable energy are non-autonomous, especially in the context of desiring to use the full potential of renewable resources. More importantly, the knowledge about the critical rate implies the necessity of devising an effective control strategy using AI technology to restrict the operation within the stable operational regime. In the future, we intend to determine the stability regimes of multi-machine power systems by incorporating the non-autonomous nature.

ACKNOWLEDGMENTS

J.K. acknowledges the financial support of the EPICC project (18-II-149-Global-A-Risikovorhersage) funded by the BMU. E.S. acknowledges the financial support of the Russian Foundation for Basic Research (RFBR) (No. 20-07-01071 A)

DATA AVAILABILITY

The data that support the findings of this study are available from the corresponding author upon reasonable request.

REFERENCES

[1]S. Pahwa, C. Scoglio, and A. Scala, "Abruptness of cascade failures in power grids," Sci. Rep. **4**, 3694 (2014).
[2]P. Hines, J. Apt, and S. Talukdar, "Large blackouts in North America: Historical trends and policy implications," Energy Policy **37**, 5249–5259 (2009).
[3]P. Kundur, N. J. Balu, and M. G. Lauby, *Power System Stability and Control* (McGraw-Hill, New York, 1994), Vol. 7.
[4]H. Ren and D. Watts, "Early warning signals for critical transitions in power systems," Electric Power Syst. Res. **124**, 173–180 (2015).
[5]P. J. Menck, J. Heitzig, N. Marwan, and J. Kurths, "How basin stability complements the linear-stability paradigm," Nat. Phys. **9**, 89 (2013).
[6]J. Ma, Y. Sun, X. Yuan, J. Kurths, and M. Zhan, "Dynamics and collapse in a power system model with voltage variation: The damping effect," PloS One **11**, e0165943 (2016).
[7]S. H. Strogatz, *Nonlinear Dynamics and Chaos: With Applications to Physics, Biology, Chemistry, and Engineering* (CRC Press, 2018).
[8]W. Ji and V. Venkatasubramanian, "Hard-limit induced chaos in a fundamental power system model," Int. J. Electr. Power Energy Syst. **18**, 279–295 (1996).
[9]S. T. Mohyud-Din and M. A. Noor, "Homotopy perturbation method for solving fourth-order boundary value problems," Math. Probl. Eng. **2007**, 98602 (2007).
[10]V. Ajjarapu and B. Lee, "Bifurcation theory and its application to nonlinear dynamical phenomena in an electrical power system," IEEE Trans. Power Syst. **7**, 424–431 (1992).
[11]I. Dobson, "Observations on the geometry of saddle node bifurcation and voltage collapse in electrical power systems," IEEE Trans. Circuits Syst. I: Fundam. Theory Appl. **39**, 240–243 (1992).
[12]B. Schäfer, D. Witthaut, M. Timme, and V. Latora, "Dynamically induced cascading failures in power grids," Nat. Commun. **9**, 1975 (2018).
[13]G. Revel, A. E. Leon, D. M. Alonso, and J. L. Moiola, "Bifurcation analysis on a multimachine power system model," IEEE Trans. Circuits Syst. I: Regul. Pap. **57**, 937–949 (2010).
[14]P. J. Menck, J. Heitzig, J. Kurths, and H. J. Schellnhuber, "How dead ends undermine power grid stability," Nat. Commun. **5**, 3969 (2014).
[15]S. M. Baer, T. Erneux, and J. Rinzel, "The slow passage through a Hopf bifurcation: Delay, memory effects, and resonance," SIAM J. Appl. Math. **49**, 55–71 (1989).
[16]A. Majumdar, J. Ockendon, P. Howell, and E. Surovyatkina, "Transitions through critical temperatures in nematic liquid crystals," Phys. Rev. E **88**, 022501 (2013).
[17]P. Ashwin, S. Wieczorek, R. Vitolo, and P. Cox, "Tipping points in open systems: Bifurcation, noise-induced and rate-dependent examples in the climate system," Phil. Trans. R. Soc. A **370**, 1166–1184 (2012).
[18]J. Tony, S. Subarna, K. Syamkumar, G. Sudha, S. Akshay, E. A. Gopalakrishnan, E. Surovyatkina, and R. I. Sujith, "Experimental investigation on preconditioned rate induced tipping in a thermoacoustic system," Sci. Rep. **7**, 5414 (2017).
[19]K. S. Suchithra and E. A. Gopalakrishnan, "Rate dependent transitions in power systems," in *2018 International Conference and Utility Exhibition on Green Energy for Sustainable Development (ICUE)* (IEEE, 2018), pp. 1–5.
[20]K. Sharafutdinov, L. Rydin Gorjão, M. Matthiae, T. Faulwasser, and D. Witthaut, "Rotor-angle versus voltage instability in the third-order model for synchronous generators," Chaos **28**, 033117 (2018).
[21]E. H. Abed and P. P. Varaiya, "Nonlinear oscillations in power systems," Int. J. Electr. Power Energy Syst. **6**, 37–43 (1984).
[22]E. M. Izhikevich, "Equilibrium," Scholarpedia **2**, 2014 (2007).
[23]S. Mariappan, R. I. Sujith, and P. J. Schmid, "Experimental investigation of non-normality of thermoacoustic interaction in an electrically heated Rijke tube," Int. J. Spray Combustion Dyn. **7**, 315–352 (2015).
[24]J. W. Bialek, "Why has it happened again? Comparison between the UCTE blackout in 2006 and the blackouts of 2003," in *2007 IEEE Lausanne Power Tech* (IEEE, 2007), pp. 51–56.
[25]Y. Hasegawa and Y. Ueda, "Global basin structure of attraction of two degrees of freedom swing equation system," Int. J. Bifurcat. Chaos **9**, 1549–1569 (1999).
[26]S. O. Blume and G. Sansavini, "Effects of stressor characteristics on early warning signs of critical transitions and "critical coupling" in complex dynamical systems," Chaos **27**, 121101 (2017).
[27]E. Cotilla-Sanchez, P. D. Hines, and C. M. Danforth, "Predicting critical transitions from time series synchrophasor data," IEEE Trans. Smart Grid **3**, 1832–1840 (2012).
[28]J. Cidras and A. E. Feijoo, "A linear dynamic model for asynchronous wind turbines with mechanical fluctuations," IEEE Trans. Power Syst. **17**, 681–687 (2002).
[29]A. Fruchard, "Canards discrets," C. R. Acad. Sci. S'er. 1 Math. **307**, 41–46 (1988), http://pascal-francis.inist.fr/vibad/index.php?action=getRecordDetail&idt=7778869.
[30]M. Egmont-Petersen, D. de Ridder, and H. Handels, "Image processing with neural networks—A review," Pattern Recognit. **35**, 2279–2301 (2002).
[31]I. Kamwa, R. Grondin, V. Sood, C. Gagnon, V. T. Nguyen, and J. Mereb, "Recurrent neural networks for phasor detection and adaptive identification in power system control and protection," IEEE Trans. Instrum. Meas. **45**, 657–664 (1996).
[32]Q. Huang, R. Huang, W. Hao, J. Tan, R. Fan, and Z. Huang, "Adaptive power system emergency control using deep reinforcement learning," IEEE Trans. Smart Grid **11**, 1171–1182 (2020).